Zwawi HAMADOUCHE[1], Mounir KHIAT[1], Abdelkader CHAKER[1]

SCAMRE LABORATORY, Department of Electrical Engineering, National Polytechnic School-Maurice Audin- Oran. BP 1523 El' M'naouer, Oran, Algeria. (1)

doi:10.15199/48.2022.06.27

Nonlinear controllers design for plug-in hybrid electric vehicle

Abstract. *Alternative options for producing electricity and fulfilling the increasing electric vehicles power demand can help in minimizing the global warming impact. It is important to maintain the load-balance generation based on load demands. This research investigates plug-in hybrid electric vehicles (PHEVs) through designing the charging and the working controllers and studying them. The DC bus voltage regulation and tracking of the battery and supercapacitor currents to their desired values were designed using non-linear sliding mode controllers. The validation of the SMC controller's efficient performance was carried out using a non-linear based backstepping controller and compared with the non-linear sliding mode controllers. Further, this research presents a comparative analysis, that is, a detailed response of the non-linear based backstepping controller and the SMC controller regarding their ability to track, the DC bus voltage regulation and desired reference, the battery, and supercapacitor currents. Also, a Lyapunov function candidate was used to analyze the PHEV's global asymptotic stability. After verification of the designed controllers using MATLAB/Simulink, the results indicate that both controllers achieved the aim of the DC bus voltage regulation and its reference voltage tracking under different load conditions.*

Streszczenie. *Alternatywne opcje wytwarzania energii elektrycznej i zaspokojenia rosnącego zapotrzebowania na energię pojazdów elektrycznych mogą pomóc w zminimalizowaniu wpływu globalnego ocieplenia. Ważne jest, aby utrzymać generowanie równoważenia obciążenia na podstawie wymagań obciążenia. W ramach tych badań badane są hybrydowe pojazdy elektryczne typu plug-in (PHEV) poprzez projektowanie ładowania i kontrolerów pracy oraz ich badanie. Za pomocą nieliniowych regulatorów trybu ślizgowego zaprojektowano regulację napięcia szyny DC oraz śledzenie prądów baterii i superkondensatorów do ich pożądanych wartości. Walidację wydajności sterownika SMC przeprowadzono przy użyciu nieliniowego sterownika wstecznego i porównano z nieliniowymi sterownikami trybu ślizgowego. Ponadto, badanie to przedstawia analizę porównawczą, czyli szczegółową odpowiedź nieliniowego kontrolera wstecznego i kontrolera SMC pod kątem ich zdolności do śledzenia, regulacji napięcia szyny DC i pożądanego odniesienia, prądów baterii i superkondensatorów. Do analizy globalnej asymptotycznej stabilności PHEV wykorzystano również kandydata na funkcję Lapunowa. Po weryfikacji zaprojektowanych sterowników za pomocą MATLAB/Simulink, wyniki wskazują, że oba sterowniki osiągnęły cel regulacji napięcia szyny DC i śledzenia jej napięcia odniesienia w różnych warunkach obciążenia.* ***(Nieliniowa konstrukcja sterowników do hybrydowego pojazdu elektrycznego typu plug-in)***

Keywords: plug-in hybrid electric vehicles (PHEVs), sliding mode controller, backstepping controller
Słowa kluczowe: hybrydowe pojazdy elektryczne typu plug-in (PHEV), kontroler trybu przesuwnego, kontroler cofania

Introduction

The use of conventional energy sources is becoming impossible as their environmental effects raise so many concerns. As a result, researchers need to find clean energy sources [1]. It is reported in [2] that C_{O2} is a major emission because of the use of conventional fuels in the transportation system and it contributes about 65 percent of global greenhouse gas (GHG) emissions. A comparison between renewable and non-renewable energy sources reveals that renewable sources emit less C_{O2}. Therefore, so much attention from stakeholders and researchers has been geared towards renewable energy sources [3].

Designing emission-free and efficient vehicle models have become very important as a result of the growing use of personal cars. With this situation in mind, several researchers have proposed the idea of fuel cell hybrid electrical vehicles (FHEVs), battery electrical vehicles (BEVs), and hybrid electric vehicles (HEV) [4].

The major part of conventional vehicles is the internal combustion engine (ICE), which runs on fossil fuel. Although the ICE has witnessed several enhancements over the years, its continued use of fossil fuels presents many negative environmental impacts. One of the main shortcomings of using fossil fuels is the emission of GHG. The idea of a hybrid vehicle was initially proposed by the German scientist, Dr. Ferdinand Porsche in 1898. The concept of a hybrid vehicle means that the vehicle is powered by two or more power sources, for example, ICE, fuel cell (FC), supercapacitor (SC), and battery. One of the main advantages of a hybrid vehicle is the improvement in fuel economy and regenerative braking. There are the major kinds of hybrid vehicles categorized according to the combination of power sources [4].

In today's market, the widely available electric vehicles (EVs) are the Plug-in EVs due to the widely available charging stations. For example, the number of charging stations in Europe and America is many. In America and Europe, vehicle charging stations are common and large in number. All Plug-in EVs need an external source to charge their electric storage system. These EVs may be based on a storage system only or hybrid with an ICE. The PHEVs have two operating modes: the charging and discharging modes. The charging mode is as the grid to vehicle (G2V) while the discharging mode is referred to as vehicle to grid (V2G). The most important part of a PHEV is the energy storage system. The most common storage systems are the supercapacitor and battery. In the design of the proposed system, the features of a supercapacitor and a battery, which make them suitable in the proposed system. For example, supercapacitors have a long life cycle and batteries have high power density. The PHEV structures can be divided into various categories.

Globally, there is a deviation of attention from non-renewable energies to renewable energies due to the large depletion of fossil fuels. Energy production from renewable energy is environmentally friendly. The use of vehicles powered by internal combustion engines is the primary cause of pollution in the environment. This pollution needs to be controlled. It is for this reason that supercapacitor and battery-based vehicles are gradually replacing ICE-based vehicles. Further, as a result of the fast growth in energy demand caused by the growing global population, storage systems made of hybrid energy sources such as supercapacitors, batteries, and fuel cells are becoming increasingly popular. PHEVs can reduce fuel consumption and pollution into the environment. Additionally, due to the potential provision of more mileage resulting from enhanced PHEV efficiency, the charge time is less and the discharge time is more through the design of an effective robust nonlinear controller. This literature presents the various types of control approaches, which are available to control PHEVs. These control approaches include backstepping control and its variants along with synergetic control, model predictive control, and nonlinear control techniques which include sliding mode control and its variants, linear control techniques which include PID control, and artificial intelligence-based control approaches

which include fuzzy logic control.

Primarily, the major aim for a PHEV control design is balance and power flow maintenance between the load and energy storage units. The authors in [5, 6], introduced a fast expansion in energy demands as an attractive issue for researchers. The outcome indicated that as a result of the use of non-renewables, the world is being faced with ozone layer depletion and environmental degradation. In [7], the authors concluded that the hybrid energy storage system (HESS) is now a significant contributor towards the use of renewable energy sources. The authors in [8], have shown that it is easy to access the various HESS topologies for HEVs and the two sources are the supercapacitor and the battery. These sources are merged such that the battery is used as the main source due to its higher energy density while the supercapacitor is used as the secondary source because of its high power density.

The authors in [9], mentions that a few incoming HEVs into the market combines battery and ICEs. Nonetheless, C_{O2} emissions continue to be an issue because of the presence of ICEs in the vehicles. However, ICE-based vehicles are being replaced by HEVs. In [10, 11], the authors proposed that it is worthwhile to use PHEVs as long as the batteries are charged from an outside power source, which could be a utility grid that uses G2V topology. So far, several researchers have introduced many DC-to-DC converter topologies to improve the effectiveness of battery charging in PHEVs.

However, if the PHEV is giving out more power than needed, it can be sent to the utility grid using the V2G technique. The authors in [12], presented how the charging of the PHEV works. In the papers, two converters were used in the PHEV charger. The first converter is a booster connected to the bridge rectifier for rectification. The second converter is the DC-to-DC converter, which varies the voltage level to direct the DC bus voltage based on the load demands.

In [13], the authors considered the use of different types of converters to charge the PHEVs. The results reveal that because the chargers are only used for battery charging, only unidirectional DC-DC converters are used.

In [14], the authors studied the battery-FC-SC based HEV energy management, which uses the fuzzy logic control with the flatness based control method. Nonetheless, a vigorous control method to achieve an effective energy distribution but is not present in this paper. In [15], the authors presented a comprehensive study of a HESS together with a sustainable power source for smart grid applications. The result revealed that the system does not have a control framework topology to manage the energy sources.

For the stability of PHEV voltage, three major control approaches are designed [16].

1. Decentralized control design
2. Centralized control design
3. Distributed control design

System Modeling

The proposed system's electric circuitry comprises a supercapacitor and battery connected via power converters (tow buck-boost converters) to a DC bus. Then, the DC bus is connected to a DC-AC inverter that drives the traction motor. An ideal HESS is supposed to be highly efficient, and have a long life cycle and high power density. There are two modes for the PHEV: the working and charging modes. Each mode needs to have a separate controller. However, finalizing the system structure of the PHEV is very important before the controller is designed. The PHEV model was finalized after the literature review was completed. Figure 1 presents the PHEV charging unit. The primary supply is coming from the main grid and a rectification circuit converts the AC to DC. The PHEV battery system possesses a specific rated voltage for charging therefore the charging is done via a buck converter. In the charging station, the charging port is connected to the charging unit of the DC bus. So, in this system, the controller will be designed to preserve the needed charging voltage level via a buck converter switch.

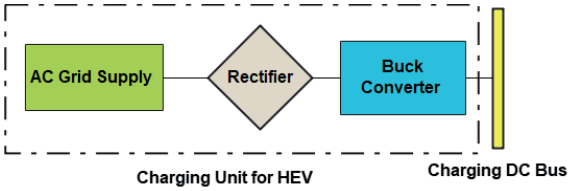

Fig. 1. Charging Stage of PHEV

Figure 2 presents the PHEV block flow diagram. In this system, the hybrid energy storage system uses a battery and supercapacitor to power the vehicle's AC motor. The benefit of the HESS is the large storage capacity, high current density, and high power density.

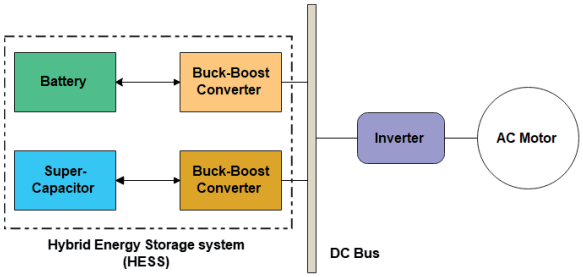

Fig. 2. Block Diagram of PHEV

Battery Model

Circuits and equations have been used to represent the battery's dynamic modeling. The equation below shows the mathematical representation of the battery model.

$$E = E_o - K\frac{Q}{Q - it} + Aexp(-B.it) \tag{1}$$

$$V_{bat} = E - R.i \tag{2}$$

These equations represent the non-linear battery model. Figure 3 below presents the battery model's circuit diagram.;

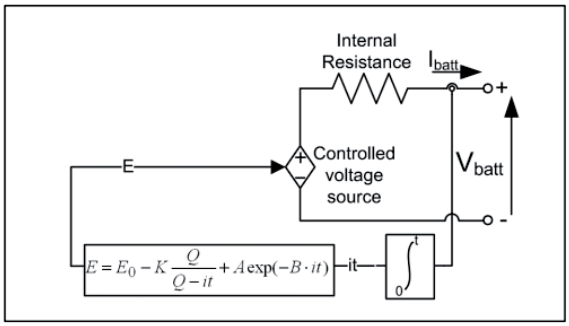

Fig. 3. Circuit Diagram of nonlinear battery model

Where V_{bat}, R, i and A represent the battery voltage, resistance, battery current and exponential zone amplitude respectively. Figure 4 illustrates the phenomena for discharging and charging the PHEV.

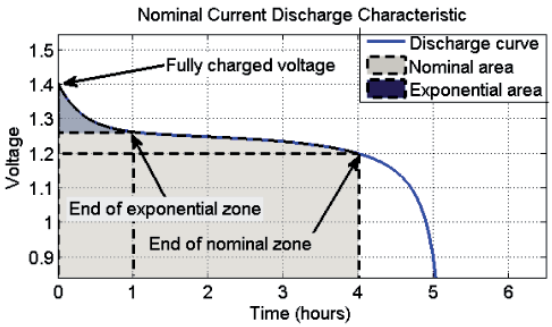

Fig. 4. Charging-Discharging Curve

In this system model design, a few assumptions were made. For example, one of the assumptions is that the circuit's internal resistance is always constant. The system parameters are obtained from the discharging phase and these parameters are used for other phases. Temperature does not affect the parameters of the system. The phenomena for charging and discharging the PHEV are dependent on the battery's state of charge (SOC). In PHEVs, the battery behavior is studied using the dynamic battery model.

SuperCapacitor Model

In the design of EVs, studying the supercapacitor model is very important. In a hybrid energy storage system, the supercapacitor serves as a storage device. In literature, several supercapacitor models have been introduced. Figure 5 shows a diagrammatical representation of the circuit diagram of a supercapacitor model. In EVs, the operation of a supercapacitor is dependent on the SOC of the supercapacitor. The equation below represents the SOC of the supercapacitor.

$$SoC_{SC} = SoC_{SCinitial} - \frac{1}{3600C_N}\int \theta_4 dt \tag{3}$$

Where θ_4 denotes the current of the supercapacitor.

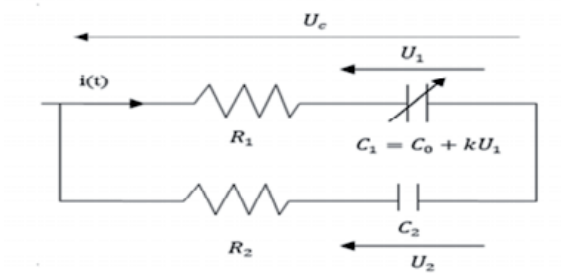

Fig. 5. Supercapacitor Model

Charger Model

Figure 1 presents the charging configuration of the PHEV charger and shows the charging units components. The rectifier circuitry comprises a full bridge rectifier followed by a capacitor, switch, diode, and inductor for controlling the output voltage based on the load demand. The rectifier output is sent to the buck converter as the AC grid supply sends a large voltage that needs to be stepped down based on the vehicle's load demand. The modeling of the buck converter voltage and current is presented below.

$$\frac{dI_{L_1}}{dt} = \frac{V_i}{u_1} - \frac{V_o}{L_1} \tag{4}$$

$$\frac{dV_o}{dt} = \frac{I_{L_1}}{C_1} - \frac{V_o}{R_1 C_1} \tag{5}$$

where I_{L_1} and V_o denote the inductor current and output voltage from the buck converter and u_1 denote the control input to the plant model.

Battery with buck-boost model

The functions of the battery include supplying load power when full and charging when the load demand and the battery's SOC is low. It is for this reason that a buck-boost converter is connected to the battery. A buck-boost converter operates in two modes: during the battery charging mode and discharging mode. The buck-boost converter has two switches: the S_1 and S_1. The $(i_{bref} > 0)$, S_1 is OFF when the SOC is high and the battery is discharging and S_2 is either ON or OFF. Conversely, for the charging mode, On the other hand for the charging mode, the $(i_{bref} < 0)$, S_2 turns OFF when the SOC is low and S_1 is either OFF or ON. The equation below explains the mathematical representation of the scenario mentioned above.

$$i_{bref} > 0 \tag{6}$$

$$\frac{di_b}{dt} = \frac{1}{L_2}v_b - \frac{R_2}{L_2}i_b - \frac{1-u_2}{L_2}v_{DC} \tag{7}$$

In equation 7, v_b and i_b represents the voltage and current of the battery respectively. Here, u_2 represents the control input given to the switch S_1.
Similarly, the equation below represents the charging mode mathematical relation.

$$i_{bref} < 0 \tag{8}$$

$$\frac{di_b}{dt} = \frac{1}{L_2}v_b - \frac{R_2}{L_2}i_b - \frac{u_3}{L_2}v_{DC} \tag{9}$$

In equation 9, u_3 represents the control input given to the switch S_2. The combined battery connected with the buck-boost model can be given after the combination of the equations (7-9) as shown below:

$$u_{23} = \begin{cases} 1-u_2 & i_{bref} > 0 \\ u_3 & i_{bref} < 0 \end{cases} \tag{10}$$

$$\frac{di_b}{dt} = \frac{1}{L_2}v_b - \frac{R_2}{L_2}i_b - \frac{u_{23}}{L_2}v_{DC} \tag{11}$$

In the equation above, 11, u_{23} denotes the average control input sent to the buck-boost battery converter.

Super-Capacitor with Buck-Boost model

A buck-boost converter was attached to the supercapacitor for the same charging and discharging. Also, the equation, which describes this is the same as the equations described in the preceding sections as shown below:

$$u_{45} = \begin{cases} 1-u_4 & i_{scref} > 0 \\ u_5 & i_{scref} < 0 \end{cases} \tag{12}$$

$$\frac{di_{sc}}{dt} = \frac{1}{L_3}v_{sc} - \frac{R_3}{L_3}i_{sc} - \frac{u_{45}}{L_3}v_{DC} \tag{13}$$

In equation 13, i_{scref} denotes the reference supercapacitor current, i_{sc} and v_{sc} represent the supercapacitor current and voltage respectively. In this converter model, u_{45} denotes the average control signal, which the switches use to control the output current.

Combined mathematical model of PHEV

The PHEV model's global mathematical representation was achieved after using Kirchhoff's current law in the output and input currents. The following model was obtained:

$$\frac{d_{v_{DC}}}{dt} = \frac{u_{23}}{C_o} i_b + \frac{u_{45}}{C_o} i_{sc} - \frac{1}{C_o} i_o \tag{14}$$

In equation 14, i_o denotes the load current. A global mathematical model may be found by joining equations (5), (11), (13) and (14), as:

$$\frac{dI_{L_1}}{dt} = \frac{V_i}{u_1} - \frac{V_o}{L_1} \tag{15}$$

$$\frac{dV_o}{dt} = \frac{I_{L_1}}{C_1} - \frac{V_o}{R_1 C_1} \tag{16}$$

$$\frac{di_b}{dt} = \frac{1}{L_2} v_b - \frac{R_2}{L_2} i_{bat} - \frac{u_{23}}{L_2} v_{DC} \tag{17}$$

$$\frac{di_{sc}}{dt} = \frac{1}{L_3} v_{sc} - \frac{R_3}{L_3} i_{sc} - \frac{u_{45}}{L_3} v_{DC} \tag{18}$$

$$\frac{dv_{DC}}{dt} = \frac{u_{23}}{C_o} i_b + \frac{u_{45}}{C_o} i_{sc} - \frac{1}{C_o} i_o \tag{19}$$

In the equations above, L_1, L_2, L_3, R_1, R_2, R_3 and C_o refer to DC-to-DC converters design parameters. u_1, u_{23}, u_{45}, as mentioned in the preceding section, define the control inputs. The following variables are assigned to the model for complete representation i_{L_1}, V_o, i_b, i_{sc} and v_{DC} as θ_1, θ_2, θ_3, θ_4 and θ_5 as shown below:

$$\frac{d\theta_1}{dt} = \frac{V_i}{u_1} - \frac{\theta_2}{L_1} \tag{20}$$

$$\frac{d\theta_2}{dt} = \frac{\theta_1}{C_1} - \frac{\theta_2}{R_1 C_1} \tag{21}$$

$$\frac{d\theta_3}{dt} = \frac{1}{L_2} v_b - \frac{R_2}{L_2} \theta_3 - \frac{u_{23}}{L_2} \theta_5 \tag{22}$$

$$\frac{d\theta_4}{dt} = \frac{1}{L_3} v_{sc} - \frac{R_3}{L_3} \theta_4 - \frac{u_{45}}{L_3} \theta_5 \tag{23}$$

$$\frac{d\theta_5}{dt} = \frac{u_{23}}{C_o} \theta_3 + \frac{u_{45}}{C_o} \theta_4 - \frac{1}{C_o} i_o \tag{24}$$

Sliding Mode Controller (SMC)

The SMC functions based on the sliding surface's derivatives with which it has many benefits over the backstepping controller. These benefits include the robustness to disturbance variations and reduction in chattering phenomena. The SMC ensures both the sliding surface S convergence to zero and the finite time derivative $\dot{S}$ to zero. Figure 6 illustrates the closed-loop working of the SMC. The SMC control input was separated into two parts: the switching and nominal controls. Similar to the preceding section, the SMC model comprises the rectifier, supercapacitor, and battery equations. The output feedback is sent to the switching and nominal control. Also, based on the error, the non-linear SMC controller generates the control input u. The PHEV mathematical model is divided into two states, which are the charging and working modes.

Charging Controller

The equation below gives the PHEV working behavior in charging mode:

$$\dot{\theta_1} = \frac{V_i}{u_1} - \frac{\theta_2}{L_1} \tag{25}$$

$$\dot{\theta_2} = \frac{\theta_1}{C_1} - \frac{\theta_2}{R_1 C_1} \tag{26}$$

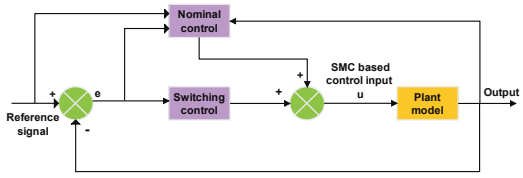

Fig. 6. Closed-loop representation of controller

As shown below, an error term is defined stating the difference between the reference charging currents and the actual charging currents to design the charging mode of the controller.

$$e_1 = \theta_1 - \theta_{1ref} \tag{27}$$

where θ_{1ref} denotes the desired state value of the charging current in the storage system of the vehicle.

$$S_1 = c_1 e_1 \tag{28}$$

where c_1 represents a constant controller gain. The time derivative of equation (28) obtains:

$$\dot{S_1} = c_1 \dot{e_1} \tag{29}$$

The following equation is produced from the time derivative of equation (29):

$$\dot{e_1} = \dot{\theta_1} - \dot{\theta}_{1ref} \tag{30}$$

Substituting the value of $\dot{q_1}$ from equation (25) in equation (65) obtains:

$$\dot{e_1} = \frac{V_i}{u_1} - \frac{\theta_2}{L_1} - \dot{\theta}_{1ref} \tag{31}$$

Replacing the value of $\dot{e_1}$ from equation (31) in equation (29) obtains:

$$\dot{S_1} = c_1 \left[\frac{V_i}{u_1} - \frac{\theta_2}{L_1} - \dot{\theta}_{1ref} \right] \tag{32}$$

The chosen control law u_1 is given as:

$$u_1 = u_{n1} + u_{s1} \tag{33}$$

where u_{s1} denotes the switching control and u_{n1} denotes the nominal control. Putting $\dot{S_1} = 0$ for finding the value of u_{n1} obtains:

$$u_{n1} = \frac{L_1}{c_1 V_i} \left(\frac{\theta_2 c_1}{L_1} + c_1 \dot{\theta}_{1ref} \right) \tag{34}$$

and

$$u_{s1} = -k_1 sgn(S_1) \tag{35}$$

Working Controller

The state-space equations of the working mode are given as:

$$\dot{\theta_3} = \frac{R_2 \theta_3}{L_2} + \frac{V_b}{L_2} - u_{23} \frac{\theta_5}{L_2} \tag{36}$$

$$\dot{\theta_4} = \frac{R_3 \theta_4}{L_3} + \frac{V_{SC}}{L_3} - u_{45} \frac{\theta_5}{L_3} \tag{37}$$

$$\dot{\theta_5} = \frac{-i_o + \theta_3 u_{23} + \theta_4 u_{45}}{C_o} \tag{38}$$

where θ_3, θ_4 and θ_5 refer to the battery current, supercapacitor current, and DC bus voltage respectively. The error terms of the working mode were defined as shown below for the controller design:

$$e_3 = \theta_3 - \theta_{3ref} \tag{39}$$

$$e_4 = \theta_4 - \theta_{4ref} \tag{40}$$

$$e_5 = \theta_5 - \theta_{5ref} \tag{41}$$

where θ_{3ref}, θ_{4ref} and θ_{5ref} represent the values of the desired state for the storage system of the vehicle. To make sure the sliding surface converges to zero, the following equation was selected:

$$S_3 = c_3 e_3 \tag{42}$$

$$S_4 = c_4 e_4 + c_5 e_5 \tag{43}$$

(44)

where c_3, c_4 and c_5 represent constant controller gains. The time derivative of equations (42) and (43) give:

$$\dot{S_3} = c_3 \dot{e_3} \tag{45}$$

$$\dot{S_4} = c_4 \dot{e_4} + c_5 \dot{e_5} \tag{46}$$

The time derivatives of equations (39), (40) and (41) yield the equations below:

$$\dot{e_3} = \dot{\theta_3} - \dot{\theta}_{3ref} \tag{47}$$

$$\dot{e_4} = \dot{\theta_4} - \dot{\theta}_{4ref} \tag{48}$$

$$\dot{e_5} = \dot{\theta_5} - \dot{\theta}_{5ref} \tag{49}$$

(50)

Substituting the value in equations (47), (48) and (49) give:

$$\dot{e_3} = \frac{R_2\theta_3}{L_2} + \frac{V_b}{L_2} - u_{23}\frac{\theta_5}{L_2} - \dot{\theta}_{3ref} \tag{51}$$

$$\dot{e_4} = \frac{R_3\theta_4}{L_3} + \frac{V_{SC}}{L_3} - u_{45}\frac{\theta_5}{L_3} - \dot{\theta}_{4ref} \tag{52}$$

$$\dot{e_5} = \frac{-I_o + \theta_3 u_{23} + \theta_4 u_{45}}{C_o} - \dot{\theta}_{5ref} \tag{53}$$

Substituting the value of $\dot{e_3}$, $\dot{e_4}$ and $\dot{e_5}$ from equations (51), (52) and (53) in equations (45) and (46) give:

$$\dot{S_3} = c_3\left(\frac{R_2\theta_3}{L_2} + \frac{V_b}{L_2} - u_{23}\frac{\theta_5}{L_2} - \dot{\theta}_{3ref}\right) \tag{54}$$

(55)

$$\dot{S_4} = c_4\left(\frac{R_3\theta_4}{L_3} + \frac{V_{SC}}{L_3} - u_{45}\frac{\theta_5}{L_3} - \dot{\theta}_{4ref}\right) + c_5\left(\frac{-I_o + \theta_3 u_{23} + \theta_4 u_{45}}{C_o} - \dot{\theta}_{5ref}\right)$$

The conclusion of the stability analysis is given in the steps below:

$$-k_3\, sgn\,(S_3) = c_3\left(\frac{R_2\theta_3}{L_2} + \frac{V_b}{L_2} - u_{23}\frac{\theta_5}{L_2} - \dot{\theta}_{3ref}\right) \tag{56}$$

(57)

$$-k_4\, sgn\,(S_4) = c_4\left(\frac{R_3\theta_4}{L_3} + \frac{V_{SC}}{L_3} - u_{45}\frac{\theta_5}{L_3} - \dot{\theta}_{4ref}\right) + c_5\left(\frac{-I_o + \theta_3 u_{23} + \theta_4 u_{45}}{C_o} - \dot{\theta}_{5ref}\right)$$

The control law u_{23} and u_{45} can be found as:

$$u_{23} = \frac{L_2}{c_3\theta_5}\left(-R_2\frac{\theta_3 c_3}{L_2} + \frac{V_b c_3}{L_2} - c_3\dot{\theta}_{3ref} + k_3\, sgn\,(S_3)\right) \tag{58}$$

$$u_{45} = \frac{L_3}{c_4\theta_5}\left(-R_3\frac{\theta_4 c_4}{L_3} + \frac{V_{UC} c_4}{L_3} - c_4\dot{\theta}_{4ref} + k_4\, sgn\,(S_4)\right) \tag{59}$$

Stability Analysis

The selected Lyapunov candidate functions for the stability analysis of the designed controllers are given below:

$$V = \frac{1}{2}S_1^2 + \frac{1}{2}S_3^2 + \frac{1}{2}S_4^2 \tag{60}$$

The time derivative of the equation above is given below:

$$\dot{V} = S_1\dot{S}_1 + S_3\dot{S}_3 + S_4\dot{S}_4 \tag{61}$$

Replacing the values of $\dot{S}_1$, $\dot{S}_3$ and $\dot{S}_4$ in the equation above gives:

$$\dot{V} = -k_1 S_1\, sgn\,(S_1) - k_3 S_3\, sgn\,(S_3) - k_4 S_4\, sgn\,(S_4) \tag{62}$$

The conclusion is given below since k_1, k_3 and k_4 are positive constants and $S_i\, sgn\,(S_i)$ is greater than zero:

$$\dot{V} \leq 0 \tag{63}$$

Backstepping Controller

The error term for the nonlinear backstepping controller design is given as:

$$e_3 = \theta_3 - \theta_{3ref} \tag{64}$$

where e_3 denotes the difference between θ_3 and θ_{3ref} represents the desired reference made available by the energy management algorithm. If the time derivative of e_3 is taken from equation (64), the result shown below is obtained:

$$\dot{e_3} = \dot{\theta_3} - \dot{\theta}_{3ref} \tag{65}$$

Now, replacing the value of $\dot{\theta_3}$ from equation (36) in equation (65), gives:

$$\dot{e_3} = \frac{R_2\theta_3}{L_2} + \frac{V_b}{L_2} - u_{23}\frac{\theta_5}{L_2} - \dot{\theta}_{3ref} \tag{66}$$

Since the defined error in equation (64) should approach zero, the Lyapunov candidate function is shown below:

$$V_1 = \frac{1}{2}e_3^2 \tag{67}$$

If the time derivative of V_1 is taken from equation (67), the following equation is obtained:

$$\dot{V_1} = e_3\dot{e_3} \tag{68}$$

$$\dot{V_1} = e_3\left[\frac{R_2\theta_3}{L_2} + \frac{V_b}{L_2} - u_{23}\frac{\theta_5}{L_2} - \dot{\theta}_{3ref}\right] \tag{69}$$

Now, we assume:

$$\dot{e_3} = -q_3 e_3 \tag{70}$$

Putting the form equation (70) yields:

$$\dot{V_1} = -q_3 e_3^2 \leq 0 \tag{71}$$

The equation changes to:

$$\frac{R_2\theta_3}{L_2} + \frac{V_b}{L_2} - u_{23}\frac{\theta_5}{L_2} - \dot{\theta}_{3ref} = -q_3 e_3 \tag{72}$$

$$\theta_5 = \frac{L_2}{u_{23}}\left(q_3 e_3 - \frac{R_2}{L_2}\theta_3 + \frac{1}{L_2}v_b - \dot{\theta}_{3ref}\right) \tag{73}$$

Taking θ_5 as α representing the virtual control law, which will be used as a reference, we obtain:

$$\alpha = \frac{L_2}{u_{23}}\left(q_3 e_3 - \frac{R_2}{L_2}\theta_3 + \frac{1}{L_2}v_b - \dot{\theta}_{3ref}\right) \tag{74}$$

Now, α becomes the reference to be tracked by θ_5 so the expression becomes:

$$e_4 = \theta_5 - \alpha \tag{75}$$

$$\theta_5 = e_4 + \alpha \tag{76}$$

Replacing the value of θ_5 in the $\dot{\theta}_5$, we obtain:

$$\dot{V_1} = e_3(-e_4 - q_3 e_3) \tag{77}$$

$$\dot{V_1} = -e_3 e_4 - q_3 e_3^2 \tag{78}$$

The equation (77) changes to the new error, which the Lyapunov candidate function for the stability analysis can use.
If the time derivative of the equation (75) is taken, we obtain:

$$\dot{e_4} = \dot{\theta_5} - \dot{\alpha} \tag{79}$$

Replacing $\dot{\theta}_5$ values in the above equation, we obtain:

$$\dot{e_4} = \frac{-i_o + \theta_3 u_{23} + \theta_4 u_{45}}{C_o} - \dot{\alpha} \tag{80}$$

Now, defining a new error to determine the control law u_{45} and taking its time derivative, the following results will be obtained:

$$e_5 = \theta_4 - \theta_{4ref} \tag{81}$$

$$\dot{e_5} = \dot{\theta_4} - \dot{\theta}_{4ref} \tag{82}$$

Now, defining another Lyapunov candidate function as shown below:

$$V_2 = \frac{1}{2}e_5^2 \tag{83}$$

If the time derivative of V_2 is taken from equation (83), we get:

$$\dot{V_2} = e_5 \dot{e_5} \tag{84}$$

$$\dot{V_2} = e_5(\dot{\theta_4} - \dot{\theta}_{4ref}) \tag{85}$$

$$\dot{V_2} = e_5\left[\frac{R_3\theta_4}{L_3} + \frac{V_{SC}}{L_3} - u_{45}\frac{\theta_5}{L_3} - \dot{\theta}_{4ref}\right] \tag{86}$$

Now, we assume:

$$\dot{e_5} = -q_5 e_5 \tag{87}$$

$$\frac{R_3\theta_4}{L_3} + \frac{V_{SC}}{L_3} - u_{45}\frac{\theta_5}{L_3} - \dot{\theta}_{4ref} = -q_5 e_5 \tag{88}$$

Now, the control law u_{45} is obtained as shown below:

$$u_{45} = \frac{L_3}{\theta_5}\left[\frac{R_3\theta_4}{L_3} + \frac{V_{SC}}{L_3}\frac{\theta_5}{L_3} - \dot{\theta}_{4ref} + q_5 e_5\right] \tag{89}$$

We perform the following steps to determine the unknown control law u_{23}:

$$V = V_1 + V_3 \tag{90}$$

$$\dot{V} = \dot{V_1} + \dot{V_3} \tag{91}$$

Replacing the $\dot{V_1}$ and $\dot{V_3}$ values, the following result is obtained:

$$\dot{V} = -e_3 e_4 - q_3 e_3^2 + e_4 \dot{e}_4 \tag{92}$$

$$\dot{V} = -q_3 e_3^2 + e_4(\dot{e}_4 - e_3) \tag{93}$$

Now, taking:

$$\dot{e}_4 - e_3 = -q_4 e_4 \tag{94}$$

Replacing the $\dot{e}_4$ values in the equation above gives:

$$\dot{e_4} = \frac{-i_o + \theta_3 u_{23} + \theta_4 u_{45}}{C_o} \quad \dot{\alpha} - e_3 = -q_4 e_4 \tag{95}$$

The final control law u_{23} is obtained as given below:

$$u_{23} = \frac{C_o}{\theta_3}\left[-\frac{i_o}{C_o} - \frac{\theta_4 u_{45}}{C_o} + \dot{\alpha} + e_3 - q_4 e_4\right] \tag{96}$$

Results and Analysis

This research conducts the design of a backstepping controller and SMC to achieve the desired control objectives. In this paper, the adopted approach is the distributed control technique where the local controller provides a constant voltage for the DC bus while tracking the reference values. The design of the SMC controller for the PHEV follows two stages. The working phase controller enables the PHEV to operate smoothly while the charger controller enables the vehicle charging.

Charging stage controller Results

The rectifier converts the AC voltage from the grid/power station into DC voltage in the charging stage. Next, the converted DC voltage is used to charge the vehicle via the buck converter. The control algorithm of the SMC is robust and can easily deal with external disturbances.

The chargers for EVs are of different types. This study considers the reference charging current of 16 A. The simulation of the closed-loop system was carried out for 10 second.

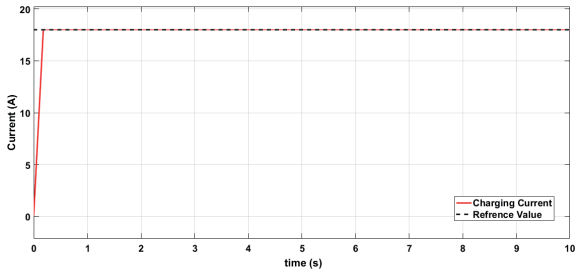

Fig. 7. Charging current θ_1 response (SMC Controller)

The figures 7 and 8 display the charging current and voltage of EV charger, respectively. From the figures, it is clear that the charger current tracks the desired value. It is

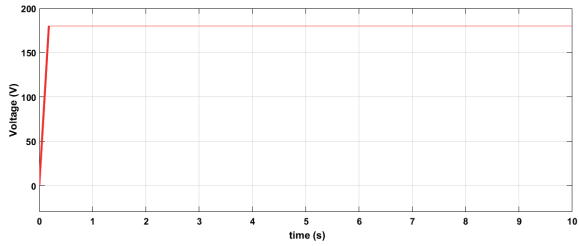

Fig. 8. Charging voltage θ_2 response (SMC controller)

possible to alter the charger reference value based on the requirement. Nonetheless, the results reveal that the controller tracks the reference value. Also, the charging voltage is within safe limits.

Working stage controller results

In the working stage, the HESS system is used to run the electric motor of the vehicle. The motor is connected to the DC bus through an inverter. The controller has been designed for the smooth working of the vehicle during different load conditions.

The obtained desired control objectives were verified using the results recorded. Figure 9 presents a graph of the load current. The load current has a direct relationship with the speed of the vehicle. This project considers a generalized load profile.

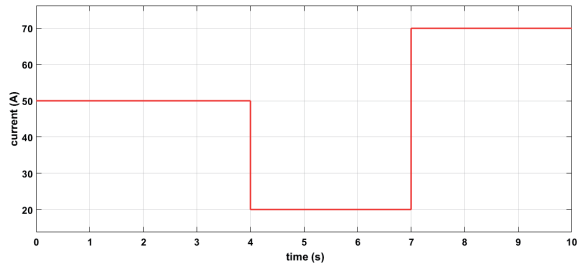

Fig. 9. Vehicle load current

The first step in the graph shows a 50 A value representing a medium speed. The second step represents a low vehicle speed while the third step denotes a high vehicle speed. The results of battery current, SC current and DC bus voltage under SMC controller are presented in figures 10, 11 and 12, respectively.

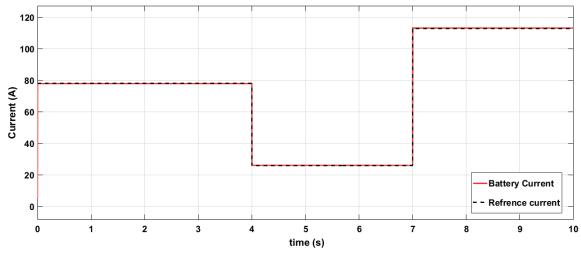

Fig. 10. Battery current θ_3 response in closed-loop

The results of the simulation indicates that the optimal values are being tracked by the DC bus voltage, supercapacitor current, and battery current. The current graph does not display any undershoot or overshoot and shows a near-zero steady-state error. Nonetheless, the DC bus voltage shows a few undershoots and overshoots caused by very fast changes in the load current. However, the response indicates that the controller has a better performance and returns the trajectory to the reference values.

The performance of the controller can be concluded as satisfactory based on the results obtained. In this research, each desired control objective has been obtained. Table 1

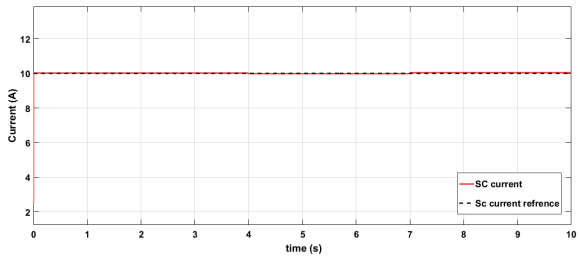

Fig. 11. SC current θ_4 response in closed-loop

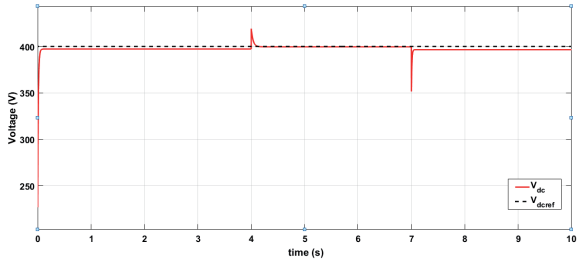

Fig. 12. DC bus voltage θ_5 response in closed-loop

shows the values of the controller gains and DC-to-DC converters parameters.

Table 1. PHEV designed converter parameters

DC-DC converters parameters	
L_1, L_2, L_3	20 mH, 20 mH
R_1, R_2, R_3	20 $m\Omega$, 20 $m\Omega$, 20 $m\Omega$
C_1, C_o	68 μF, 68 μF
Switching frequency	100 kHz
PHEV controller gains	
c_1, c_3, c_4, c_5	0.1, 0.1, 0.5
k_1, k_3, k_4	1000, 1000, 1000

Backstepping Controller Results

A comparative analysis for the backstepping-based nonlinear controller. The backstepping controller uses a recursive method where the virtual control laws alongside the actual control inputs are derived. The implementation of the backstepping controller has been done for the operating stage of the electric vehicle. The values and parameters of the backstepping controller remain the same as those of the SMC for effective comparison. Figure 13 presents the backstepping controller battery current response. The current response is shown in the red line. The black dotted lines represent the reference values.

From the figure, it is seen that the battery current tracks the reference. Nonetheless, the backstepping controller does not appropriately handle the value changes and suspends the tracking momentarily revealing that the controller is not robust. However, the backstepping controller can be utilized if the system can withstand this shortcoming.

Similarly, the figures 14 and 15 respectively show the supercapacitor current and voltage of the DC bus. From the above figures, it can be seen that the current of the supercapacitor tracks nicely after an overshoot at 40 A. Regarding the supercapacitor, this overshoot is called transient response.

The figure 15 presents the response of the backstepping controller for the Dc bus voltage where a high overshoot was observed at 600 V indicating a poor performance for the controller. In this system, a few intolerable undershoot may be observed in the response, which is required to follow the reference voltage effectively.

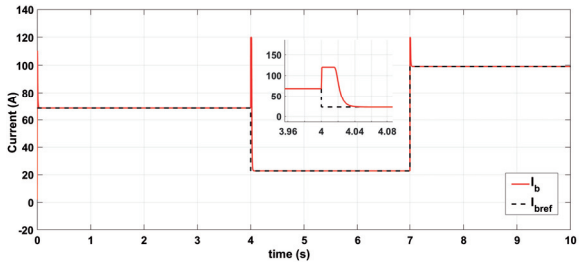

Fig. 13. Battery Current (Backstepping Response)

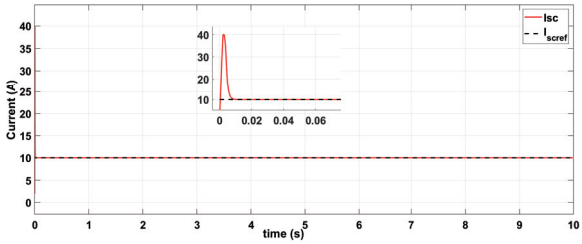

Fig. 14. Supercapacitor Current (Backstepping Response)

Comparative Analysis

To validate the SMC controller performance, a comparison between the backstepping and SMC controllers regarding the voltage of the DC bus has been presented. Figure 16 shows the responses obtained from these controllers for regulating the voltage of the DC bus. The responses are presented in zoomed-in views. Noteworthy to notice is the undershoot voltage (320 V) and overshoots (600 V), which the backstepping controller exhibits. The SMC exhibits minute undershoots and overshoots and perfectly matches the 400 V DC bus voltage by SMC are very minute and follows the reference of 400V perfectly.

Conclusion

This paper investigated the design and control of a plug-in hybrid electric vehicle (PHEV). Two units of the PHEV have been discussed in this work – the working and charging units. The charging unit comprises a rectifier. The rectifier performs the conversion of the AC voltage into a DC voltage for the buck converter. The bulk converter steps down the high AC voltage from the power station so that the HEV can utilize it. The second unit of the PHEV comprises a hybrid energy storage system (HESS) made up of a supercapacitor and a battery. The HESS functions as a load-balance generation where the supercapacitor works as the secondary source and the battery works as the primary source. The sliding mode controller (SMC) was designed to control the working and charging units currents and regulate the voltage of the DC bus indirectly. The proposed methodology enables the charging unit and the HESS to satisfy the load demands via efficient power management. In addition, the Lyapunov stability analysis was used to verify the system's global stability as the Lyapunov candidate derivative function was obtained

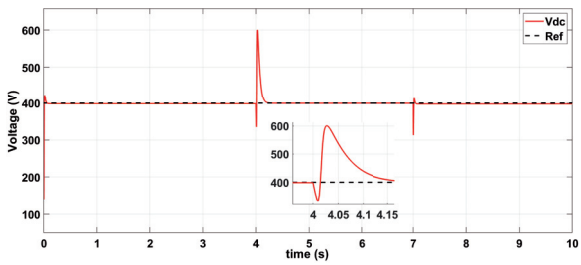

Fig. 15. DC bus voltage regulation (Backstepping Response)

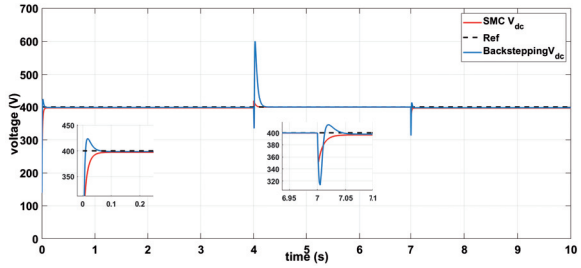

Fig. 16. DC bus voltage comparison between SMC and backstepping controller

as negative. The simulation was divided into different parts: closed-loop and open-loop analyses. The open-loop analysis uses MATLAB/Simulink to analyze the system's uncontrolled response. The closed-loop uses MATLAB/Simulink to simulate the designed SMC controllers to verify the performance of the designed framework. The non-linear backstepping controller was compared with the SMC controllers to determine the SMC controller's effective performance. The comparison revealed that the SMC controller functions perfectly for the system while the backstepping controller exhibited largely undershoots and overshoots, therefore, the backstepping controller exhibits poor performance. It is evident from the work conducted that the system's response to the open-loop analysis indicate that the voltage of the DC bus was not maintained, therefore, does not work for the system. In conclusion, the results from the SMC controllers indicate that the real-time implementation and validation of this research is possible for an efficient PHEV performance.

***Authors**: MS. Zwawi Hamadouche, Prof. M. Khiat, Prof. A. Chaker, SCAMRE LABORATORY, Department of Electrical Engineering, National Polytechnic School-Maurice Audin- Oran. BP 1523 El' M'naouer, Oran, Algeria, email: hamadouche92zouaoui@gmail.com,*

REFERENCES

[1] Bilgen, S., Kaygusuz, K. and Sari, A: Renewable Energy for a Clean and Sustainable Future, Energy Sources, 26(12), pp. 1119-1129, 2004.

[2] Tutor, M.A: The documentation on how the data was transformed was, tutordocumentation United States Environmental Protection Agency, [web page] http://www.epa.gov/ghgemissions/.

[3] Shafiei, S. and Salim, R.A.: Non-renewable and renewable energy consumption and CO2 emissions in OECD countries: A comparative analysis, Energy Policy, 66, pp. 547-556, 2014.

[4] Chan, C. C.: The state of the art of electric, hybrid, and fuel cell vehicles, Proceedings of the IEEE, 95(4), pp. 704-718, 2007.

[5] Gejguš, M., Aschbacher, C. and Sablik, J.: Comparison of the total costs of renewable and conventional energy sources, Research Papers Faculty of Materials Science and Technology Slovak University of Technology, 24(37), pp. 99-104, 2016.

[6] Dreidy, M., Mokhlis, H. and Mekhilef, S.: Inertia response and frequency control techniques for renewable energy sources: A review, Renewable and sustainable energy reviews, 69, pp. 144-155, 2017.

[7] Aneke, M. and Wang, M.: Energy storage technologies and real life applications–a state of the art review, Applied Energy, 179, pp. 350-377, 2016.

[8] Shiau, C.S.N., Samaras, C., Hauffe, R. and Michalek, J.J.: Impact of battery weight and charging patterns on the economic and environmental benefits of plug-in hybrid vehicles, Energy Policy, 37(7), pp. 2653-2663, 2009.

[9] Khan, M.S., Ahmad, I. and Abideen, F.Z.U: Output voltage regulation of fc-uc based hybrid electric vehicle using integral backstepping control, IEEE Access, 7, pp. 65693-65702, 2019.

[10] Lacroix, S., Labouré, E. and Hilairet, M.: An integrated fast battery charger for electric vehicle, in 2010 IEEE Vehicle

Power and Propulsion Conference, IEEE, 2018, pp. 1-6.
[11] Kumar, S. and Usman, A.: A review of converter topologies for battery charging applications in plug-in hybrid electric vehicles, in 2018 IEEE Industry Applications Society Annual Meeting (IAS), IEEE, 2018, pp. 1-9.
[12] Rachid, A., Fadil, H.E., Belhaj, F.Z., Gaouzi, K. and Giri, F.: Lyapunov-based control of singlephase ac–dc power converter for bev charger, in Recent Advances in Electrical and Information Technologies for Sustainable Development. , Springer, 2019, pp. 115–121.
[13] Cheng, K.W.E., Divakar, B.P., Wu, H., Ding, K. and Ho, H.F.: Battery-management system (bms) and soc development for electrical vehicles, IEEE transactions on vehicular technology, 60(1), pp. 76-88, 2010.
[14] Zandi, M., Payman, A., Martin, J.P., Pierfederici, S., Davat, B. and Meibody-Tabar, F.: Energy management of a fuel cell/supercapacitor/battery power source for electric vehicular applications, IEEE transactions on vehicular technology, 60(2), pp. 433-443, 2010.
[15] Aktas, A., Erhan, K., Ozdemir, S. and Ozdemir, E.: Experimental investigation of a new smart energy management algorithm for a hybrid energy storage system in smart grid applications, Electric Power Systems Research, 144, pp. 185-196, 2017.
[16] Kumar, J., Agarwal, A. and Agarwal, V.: A review on overall control of dc microgrids, Journal of energy storage, 21, pp. 113-138, Feb. 2019.